Engineering Geology 264 (2020) 105317

Contents lists available at ScienceDirect

Engineering Geology

journal homepage: www.elsevier.com/locate/enggeo

Coupled geotechnical-climatic design procedure for drilled shaft subjected to axial load

Vahidreza Mahmoudabadi[a,*], Nadarajah Ravichandran[b]

[a] Glenn Department of Civil Engineering, Clemson University, Clemson, SC, 29634, United States
[b] Glenn Department of Civil Engineering, Clemson University, 202 Lowry Hall, Clemson, SC 29634, United States

ARTICLE INFO

Keywords:
Drilled shaft
Climatic event
Hydrological event
Axial capacity
Partially saturated soil
Infrastructure

ABSTRACT

In this paper, a novel procedure is proposed to incorporate the site-specific hydrological/climatic parameters into the geotechnical design of drilled shaft with sample applications in Riverside, CA and Salt Lake City, UT. The variation of degree of the saturation and/or matric suction due to the hydrological/climatic events was modeled using the one-dimensional Richards' equation considering historical resultant infiltration rate and water table depth as the upper and lower boundary conditions, respectively. The historical rainfall, evapotranspiration, and water table depth were considered in a probabilistic manner to estimate a representative degree of saturation and/or matric suction in the subsurface soil that support the drilled shaft. The results indicate that the ultimate axial capacity of the drilled shaft increases by as much as 40% of the conventional fully saturated method in Salt Lake City, while this is almost 56% for Riverside, CA. In case of the settlement, the total elastic settlement of the drilled shaft decreases by almost 34% and 30% at Salt Lake City and Riverside, respectively. Also, it is observed that the water table depth, intensity, and duration of the rainfall have noticeable impacts on the design parameters of the drilled shaft.

1. Introduction

The recent records indicate that the severe hydrological/climatic events such as heavy rainfall, flood, and drought have become frequent in recent years (Trenberth, 2011). These events cause significant economic losses every year in the United States and around the world. The 2014 New York flood, 2015 Missouri flood, 2016 Oklahoma flood, 2016 Louisiana flood, 2017 California flood, and 2017 Houston flood are some of the examples of severe floods in the United States. Also, the significant part of the United States has been struggling with the severe droughts over a long period of time. The droughts happened in the North America during the 19th century, Southwestern United States (New Mexico and Texas) in 1950, and Midwest and Rocky Mountain regions in 2002 are some of the examples of severe drought in the United States. According to the National Climatic Data Centre (NCDC), 30% of the United States suffered from moderate to severe drought in recent years. These extreme hydrological/climatic events have notable damages to the above-ground structures (Steenbergen et al., 2009).

The load-bearing capacity and settlement of foundation, an interface between the above-ground structures and the subsurface soil are highly affected by the flow, deformation, and strength properties of the underlying soil. These soil properties are greatly influenced by the hydrological/climatic events through changing the saturation level of the subsurface soil. However, the impacts of hydrological/climatic events on the subsurface soil properties and subsequently the foundations that support various structures such as bridge, buildings, earth dams, and levees are ignored in the current design procedures (Schuster and Highland, 2001; Robinson et al., 2017; Turnbull, 2016). In addition, the current loss estimation schemes used by the insurance companies and other agencies simply ignore the damage caused by the foundation failures (bearing capacity and settlement) (Vardon, 2015; Moftakhari et al., 2017). Therefore, a coupled geotechnical-climatic model must be developed to predict the behavior of foundations under significant hydrological/climatic events accurately. In this study, the impacts of hydrological/climatic parameters such as rainfall, evapotranspiration, and water table depth on the ultimate load-bearing capacity and settlement of drilled shaft foundation were investigated considering site-specific hydrological/climatic parameters.

The drilled shaft is a type of deep foundation used to support superstructures and transfer the structural loads to the deeper soil through the side and bottom of the shaft (Kulhawy, 1991). The drilled shaft is commonly designed assuming that the soil is fully saturated with the water table at the ground surface even if the historical water table is well below the tip of the shaft. Recent fundamental studies on soil

* Corresponding author.
E-mail addresses: vmahmou@clemson.edu (V. Mahmoudabadi), nravic@clemson.edu (N. Ravichandran).

https://doi.org/10.1016/j.enggeo.2019.105317
Received 6 January 2019; Received in revised form 18 June 2019; Accepted 26 September 2019
Available online 31 October 2019
0013-7952/

Nomenclature

A_p	Cross-section area of shaft
A_s	Drilled shaft perimeter
A_{Tip}	Drilled shaft tip area
B	Drilled shaft diameter
C	Specific moisture capacity
$c_a^{'}$	Soil adhesion under fully saturated condition
D	Drilled shaft length
$ESAT$	Saturated vapor pressure
E_p	Modulus of elasticity of drilled shaft material
E_{soil}	Soil modulus of elasticity
$E_{soil(sat)}$	Soil modulus of elasticity under the fully saturated condition
$E_{soil(unsat)}$	Soil modulus of elasticity under partially saturated condition
e	2.718281828
e_s	Void ratio
$F_{Evapotranspiration}$	Evapotranspiration intensity
$F_{Rainfall}$	Historical rainfall intensity
$F_{Resultnat\ Infiltration}$	Resultant infiltration at upper boundary condition
F_{Runoff}	Surface runoff
f_j^{sat}	Unit skin resistance at fully saturated condition for *jth* segment
$f_j\,(u_a - u_w)$	Unit skin friction due to matric suction for *jth* segment
I_p	Plasticity index
I_{rr}	Reduced rigidity index
I_{wp}	Tip's influence factor
I_{ws}	Skin's influence factor
i	Node number
i_j	First node of *jth* segment
j	Segment number
K	Unsaturated hydraulic conductivity
$KPEC$	Calibration coefficient
K_r	Relative hydraulic conductivity
K_{sat}	Soil hydraulic conductivity under fully saturated condition
L	Pile length
L_d	Daytime length
m	Iteration level
N_q	Non-dimensional bearing capacity factor
N_γ	Non-dimensional bearing capacity factor
n	SWCC fitting parameter
n_j	Last node of *jth* segment
PET	Potential Evapotranspiration
p	Total number of shaft segment
Q_{Skin}	Drilled shaft skin resistance
$Q_j^{Skin(sat)}$	Skin resistance under fully saturated condition
$Q^{Skin}(u_a - u_w)$	Effect of matric suction on skin resistance
Q_{Tip}	Drilled shaft tip resistance
Q_{Ult}	Drilled shaft ultimate axial compression capacity
Q_{wskin}	Load carried by shaft skin under working load condition
Q_{wtip}	Load carried at the shaft tip under working load condition
q_{Tip}	Tip bearing capacity
q_{wtip}	Shaft tip load per unit area under working load condition
$RHOSAT$	Saturated vapor density
r	Number of data points
S_e	Total elastic settlement of drilled shaft
$S_{e(1)}$	Elastic settlement of drilled shaft
$S_{e(2)}$	Settlement of drilled shaft caused by a load at the shaft tip
$S_{e(3)}$	Settlement of the drilled shaft caused by a load transmitted along the shaft skin
S_j	Degree of Saturation for *jth* segment
T	Average air temperature
t	Time
$(u_a\text{-}u_w)_{avg(j)}$	Average matric suction of *jth* segment
$(u_a\text{-}u_w)_i$	Matric suction at *ith* node of soil profile
v	Data index
W	Weight of drilled shaft
x_v	Annual maximum historical rainfall or water table data
y_v	Linearized form of the cumulative density function of Gumbel distribution
z	Depth
α	SWCC fitting parameter
α_e	Fitting parameter
β_e	Fitting parameter
β_j	Burland-Bjerrum coefficient
β_n	Gumbel distribution standard deviation
γ	Unit weight of soil
γ_d	Dry soil unit weight
γ_w	Unit weight of water
$\bar{\gamma}$	Average unit weight
Δt	Time interval
Δz	Depth interval
δ'	Effective angle of interface between soil and shaft skin
θ	Volumetric water content
θ_r	Residual water content
θ_s	Saturated water content
κ	Fitting parameter
μ_n	Gumbel distribution mode
μ_s	Soil Poisson's ratio
ζ	Unit skin resistance coefficient
$\xi_{\text{-}d}$	Depth factor
$\xi_{\text{-}r}$	Soil rigidity factor
$\xi_{\text{-}s}$	Shape factor
$\sigma'_{z(j)}$	Vertical effective stress for *jth* segment
$\sigma'_{z(Tip)}$	Effective stress at the tip of the drilled shaft
ϕ'	Effective friction angle
ψ	Pressure head
$\psi_{avg(j)}$	Average pressure head of *jth* segment

mechanics indicate that the flow, deformation, and shear strength parameters of the subsurface soil are influenced by the degree of saturation and matric suction of the soil (Fredlund et al., 1978, 2012; Lu and Likos, 2004; Kulhawy and Mayne, 1990; Das, 2010; Briaud, 2013). Over the past decades, many researchers have proposed methods to consider the effect of the degree of saturation and matric suction on the hydro-mechanical behavior of soil through widely used degree of saturation-matric suction relationship called Soil Water Characteristics Curve (SWCC) (Vanapalli et al., 1996; Oberg and Sallfors, 1997; Lee et al., 2005; Garven and Vanapalli, 2006; Guan et al., 2010; Sheng, 2011). Following that, several researchers investigated the influence of matric suction on the unsaturated soil behavior and interface shear strength (Khoury et al., 2010; Borana et al., 2015, 2016). In recent years, further advancement was made to incorporate the influence of matric suction and degree of saturation on the load carrying capacity of deep and shallow foundations using plate-load tests (Douthitt et al., 1998; Georgiadis et al., 2003; Costa et al., 2003; Tariq and Miller, 2009; Vanapalli and Taylan, 2012; Mahmoudabadi and Ravichandran, 2019) and model footing tests (Vanapalli et al., 2010; Vanapalli and Oh, 2010b; Vanapalli and Taylan, 2011a, 2011b, 2012). Another group of researchers studied the impacts of matric suction on the soil stiffness (Agarwal and Rana, 1987; Steensen-Bach et al., 1987; Schnaid et al., 1995; Oh et al., 2009; Vanapalli and Oh, 2010a; Costa et al., 2003; Rojas et al., 2007; Vanapalli and Adem, 2013).

The above-mentioned studies indicate that the current foundation design procedure must be revised by incorporating the site-specific

hydrological/climatic parameters for accurately predicting the ultimate bearing capacity and settlement. Such a revision will require a clear understanding of principles that govern the hydro-mechanical behavior of partially saturated soil and access to site-specific historical rainfall, evaporation, and water table depth data. In recent years, a limited number of efforts have been undertaken to assess the influence of hydrological/climatic events on the behavior of geotechnical systems. Mahmoudabadi and Ravichandran (2017, 2019) presented a framework to take the historical rainfall and water table into account for computing the bearing capacity and elastic settlement of shallow and deep foundations. Following that, Ravichandran et al. (2017) applied the probabilistic analysis in the design process of shallow foundation in partially saturated soils. Kim et al. (2017) studied the effect of rainfall on shallow foundation settlement using numerical analysis and compared its result with in-situ load tests for low-range matric suction. Moreover, Vahedifard and Robinson (2016) proposed a unified method based on model footing and plate load tests to estimate the ultimate bearing capacity of shallow foundation in partially saturated soil considering different surface flux boundary conditions and fluctuation of water table depth.

Since none of the above-mentioned studies revised the drilled shaft design procedure, this study aims to develop a procedure for coupling site-specific hydro-climatic parameters with geotechnical parameters to compute the ultimate axial capacity and settlement of drilled shaft. This procedure is demonstrated through sample applications at two sites in the United States. To this end, first, a numerical scheme was developed to solve the one-dimensional Richards equation to capture the temporal and spatial variation of the degree of saturation and matric suction considering the resultant infiltration and water table depth as the upper and lower boundary conditions, respectively. Then, the Monte Carlo simulation technique was used to randomly generate the inputs (upper and lower boundary conditions) based on their probability distributions. Finally, the ultimate axial capacity and settlement of the drilled shafts were calculated using the equations that consider the effects of degree of saturation and/or matric suction. A parametric study was conducted to investigate the effects of rainfall duration on the computed ultimate axial capacity and settlement.

2. Coupled geotechnical-climatic design of drilled shaft

2.1. Ultimate axial capacity - safety requirement

The ultimate axial compression capacity of the drilled shaft, Q_{Ult}, was calculated using the simplified equation shown in Eq. (1) (Kulhawy and Mayne, 1990).

$$Q_{Ult} = Q_{Skin} + Q_{Tip} - W \tag{1}$$

where Q_{Skin} is the drilled shaft skin resistance, Q_{Tip} is the drilled shaft tip resistance, and W is the weight of the drilled shaft. To calculate the ultimate axial compression capacity of a drilled shaft, first, the skin and tip resistance need to be computed due to the soil matric suction and degree of saturation. The contribution of matric suction and degree of saturation towards the axial capacity of a drilled shaft in partially saturated soils has been the subject of numerous studies which were discussed in the introduction section in detail.

2.1.1. Skin resistance

Among the many empirical and semi-empirical equations available in the literature, the equation proposed by Vanapalli and Taylan (2012) was used in this study to compute skin resistance as a function of the degree of saturation and/or matric suction (Eq. (2)). The proposed equation considers the effect of matric suction in resisting the axial load along the skin, $Q^{Skin(u_a - u_w)}$, as an additive term to the conventional method that considers the soil is fully saturated, $Q_j^{Skin(sat)}$.

$$\begin{aligned} Q_{Skin} &= \sum_{j=1}^{p} \left(Q_j^{Skin(sat)} + Q_j^{Skin(u_a-u_w)}\right) = A_s \sum_{j=1}^{p} \left(f_j^{sat} + f_j^{(u_a-u_w)}\right) \\ &= \sum_{j=1}^{p} \left[c_a' + \beta_j \sigma'_{z(j)} + (u_a - u_w)_{avg(j)} (S_j^{\kappa}) \tan\delta'\right] \pi B D \end{aligned} \tag{2}$$

where j is the segment number, $f_j^{(u_a - u_w)}$ is the unit skin friction due to matric suction for jth segment, f_j^{sat} is the unit skin resistance at fully saturated condition for jth segment, A_s is the shaft perimeter, p is the total number of shaft segment, c_a' is the soil adhesion in saturated condition, β_j is the Burland-Bjerrum coefficient for jth segment which is equal to $K_o \tan\phi'$ (K_o is mean lateral earth pressure coefficient at rest equal to 1-sin(ϕ'), where ϕ' is soil effective friction angle), δ' is the effective angle of interface between soil and shaft skin that is equal to 2/3ϕ' (Tariq and Miller, 2009), $\sigma'_{z(j)}$ is the vertical effective stress for jth segment, $(u_a\text{-}u_w)_{avg(j)}$ is the average matric suction of jth segment, S_j is the degree of saturation for jth segment, B is the shaft diameter, D is the shaft length, and κ is the fitting parameter used for obtaining the best-fit between the measured and predicted value which is described in details in Vanapalli and Fredlund (2000). The average matric suction of each segment ($(u_a\text{-}u_w)_{avg(j)}$) is expressed in Eq. (3).

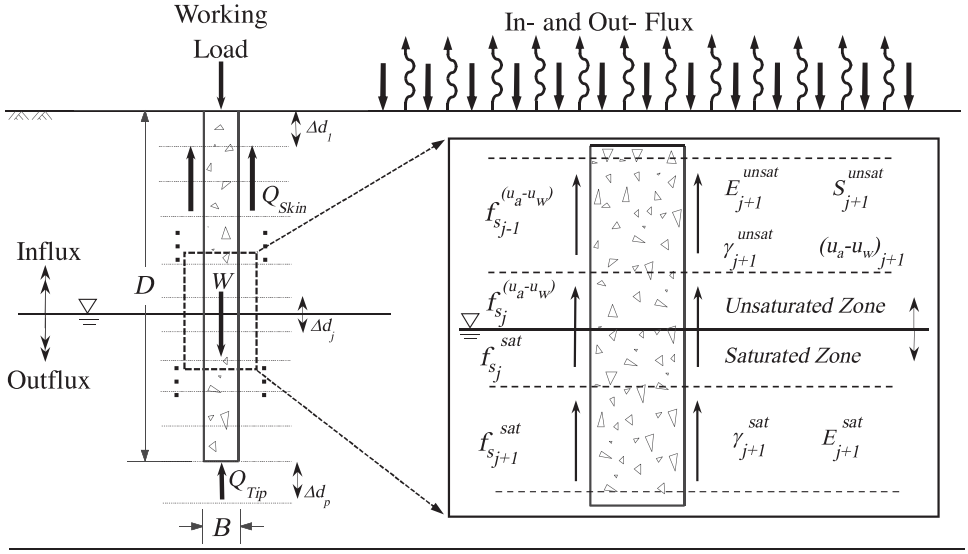

Fig. 1. Schematic of the proposed procedure for computing skin resistance (Mahmoudabadi and Ravichandran, 2019).

$$(u_a - u_w)_{ave(j)} = \frac{\sum_{i=i_j}^{n_j} [(u_a - u_w)_i]}{n_j - i_j} = -\psi_{ave(j)}\gamma_w \quad (3)$$

where $(u_a\text{-}u_w)_i$ is the matric suction at ith node of soil profile; i_j is the first node of jth segment; n_j is the last node of jth segment; $\psi_{avg(j)}$ is the average pressure head of jth segment, and γ_w is the unit weight of water. Generally, in order to calculate the total skin resistance accurately, first the drilled shaft is discretized into a number of small segments, and then the soil suction-related parameters such as the degree of saturation, matric suction, unit weight, and corresponding skin resistance are computed for each segment separately. Finally, the total skin resistance for the entire pile is calculated by summing up the skin resistance of each segment. Fig. 1 displays the schematic of the procedure for calculating the skin resistance for a deep foundation.

2.1.2. Tip resistance

The tip resistance was calculated using the equation (Eq. (4)) proposed by Kulhawy and Mayne (1990). In this method, the effect of the partially saturated soil condition is considered through the change in unit weight of the soil(γ) and also the effective stress at the tip of the pile, $\sigma'_{z(Tip)}$.

$$Q_{Tip} = q_{Tip}A_{Tip} = (0.5\bar{\gamma}BN_\gamma\xi_{\gamma s}\xi_{\gamma d}\xi_{\gamma r} + \sigma'_{z(Tip)}N_q\xi_{qs}\xi_{qd}\xi_{qr})0.25\pi B^2 \quad (4)$$

where q_{Tip} is the tip bearing capacity; A_{Tip} is the shaft tip area; $\bar{\gamma}$ is the average unit weight from depth D to $D + B$; N_γ and N_q are the non-dimensional bearing capacity factors that are functions of the effective soil friction angle, and ξ_{-s}, ξ_{-d}, *and* ξ_{-r} are the shape, depth, and soil rigidity factors, respectively. The default values and/or the equations are tabulated in Table 1. Readers are referred to Kulhawy and Mayne (1990) for further details.

2.2. Settlement (elastic) - serviceability requirement

The total elastic settlement of a drilled shaft, S_e was calculated using the Eqs. (5)–(8) (Das, 2010).

$$S_e = S_{e(1)} + S_{e(2)} + S_{e(3)} \quad (5)$$

$$S_{e(1)} = \frac{(Q_{wtip} + \zeta Q_{wskin})}{A_p E_p} \quad (6)$$

$$S_{e(2)} = \frac{q_{wtip}B}{E_{soil}}(1 - \mu_s^2)I_{wp} \quad (7)$$

$$S_{e(3)} = \left(\frac{Q_{wskin}}{A_s D}\right)\frac{B}{E_{soil}}(1 - \mu_s^2)I_{ws} \quad (8)$$

where $S_{e(1)}$ is the elastic settlement of the drilled shaft, $S_{e(2)}$ is the settlement of the drilled shaft caused by the load at the shaft tip, $S_{e(3)}$ is the settlement of the drilled shaft caused by the load transmitted along the shaft skin, Q_{wtip} is the load carried at the shaft tip under working load condition, Q_{wskin} is the load carried by shaft skin under working load condition, ζ is a coefficient which depends on the distribution of the unit skin resistance along the shaft skin and it is assumed 0.67, A_p is the cross-section area of shaft, E_p is the modulus of elasticity of the drilled shaft material (concrete), q_{wtip} is the shaft tip load per unit area under working load condition, E_{soil} is the soil modulus of elasticity, μ_s is the soil Poisson's ratio which is assumed to be 0.3, I_{wp} and I_{ws} are the tip's and skin's influence factors, respectively. I_{wp} is assumed to be 0.85 in this study and I_{ws} is equal to $2 + 0.35(L/D)^{0.5}$, where L is pile length (Das, 2010). In addition to the shear strength parameters, the soil modulus of elasticity (E_{soil}) is another parameter which is affected by the degree of saturation and matric suction of the soil profile along the shaft skin. Since the degree of saturation and the matric suction are computed following the procedure described before, the elastic settlement can be computed if E_{soil} is also expressed as a function of the degree of saturation and matric suction.

As discussed in the introduction section, various empirical equations have been proposed to predict the modulus of elasticity of the soil as a function of matric suction and/or degree of saturation. In this study, the equation proposed by Oh et al. (2009), shown in Eq. (9), was used to estimate the modulus of elasticity in partially saturated coarse-grained soils ($E_{soil(unsat)}$).

$$E_{soil(unsat)} = E_{soil(sat)}[1 + \alpha_e(u_a - u_w)_{ave}S^{\beta_e}] \quad (9)$$

where $E_{soil(sat)}$ is the soil modulus of elasticity under the saturated condition, $(u_a\text{-}u_w)_{avg}$ is the average matric suction within foundation influence zone (hereafter refers to as "average matric suction"), and α_e and β_e are fitting parameters. For coarse- and fine-grained soil, the recommended fitting parameter, β_e, is equal to 1 and 2, respectively. Also, the fitting parameter α_e depending upon the plasticity index (I_p) is computed using the following empirical equation (Eq. (10)), developed by Oh et al. (2009).

$$1/\alpha = 0.5 + 0.312(I_P) + 0.109(I_P)^2 \quad (0 \le I_P(\%) \le 12) \quad (10)$$

It should be noted that to calculate the total settlement of a drilled shaft the consolidation settlement is also required. The consolidation settlement is omitted in this study for two reasons. The first reason is that the consolidation settlement is a long-term process which usually takes years to show significant settlement especially when the foundation is supported by a fine-grained soil. However, in reality, the degree of saturation fluctuation due to a hydrological/climatic event for a short period of time and the amount of consolidation settlement will be negligible. The second reason is that the lack of well–established correlations for computing the consolidation parameters such as compression index, recompression index and preconsolidation pressure as functions of the degree of saturation and/or matric suction in the literature. When such correlations are available, one could calculate the consolidation settlement due to the variation in the degree of saturation and add it with that of primary consolidation settlement based on saturated parameters and elastic settlement. It is worth mentioning that the employed equations and selected parameters are calibrated for a mixture of coarse- and fine-grained soils with plasticity index less than 16% according to the discussed literature.

As is expressed in this section, the ultimate axial capacity and settlement of drilled shaft directly relate to the degree of saturation and matric suction of underlying soil. Thus, these parameters need to be accurately calculated for any site condition. The procedure of calculating the site-specific degree of saturation and matric suction is described in the next section.

3. Determination of spatial variation of degree of saturation and matric suction

During rainfall, water infiltrates into the ground from the ground surface and the degree of saturation in the soil changes with time. In this study, the vertical movement of water through the partially saturated soil was represented by one-dimensional Richards equation (Richards, 1931) which is shown in Eq. (11). This nonlinear partial

Table 1
Shape, depth and soil rigidity factors for circular tip resistance (Kulhawy and Mayne, 1990).

Factor	Symbol	Value/Equation
Shape	$\xi_{\gamma s}$	0.6
	ξ_{qs}	$1 + \tan\phi'$
Depth	$\xi_{\gamma d}$	1
	ξ_{qd}	$1 + 2\tan\phi'(1\text{-}\sin\phi')^2[(\pi/180)\tan^{-1}(D/B)]$
Rigidity	$\xi_{\gamma r}$	ξ_{qr}
	ξ_{qr}	$\exp\{[-3.8\tan\phi'] + [(3.07\sin\phi')(\log_{10}(2I_{rr}))/(1 + \sin\phi')]\}$

ϕ': Effective friction angle.
I_{rr}: Reduced rigidity index.

differential equation derived from Darcy's law predicts a decrease of the water infiltration for the different flux rates in the subsurface area.

$$\frac{\partial\theta}{\partial t} = \frac{\partial}{\partial z}\left[K\left(1 + \frac{\partial\psi}{\partial z}\right)\right] \tag{11}$$

where t is the time, z is the depth from the ground surface, θ is the volumetric water content, K is the unsaturated hydraulic conductivity, ψ is the pressure head, and $\frac{\partial\psi}{\partial z}$ is the hydraulic gradient. Although the problem considered in this study is three-dimensional in nature, it is assumed that the one-dimensional model is reasonably accurate to predict the vertical movement of the water for demonstrating the proposed procedure for the structures with small footprint such as bridge foundation, foundation of wind turbines, and transmission towers where the shafts are placed at corners or center of structure close to the outdoor environment (Van Dam and Feddes, 2000; Zha et al., 2013; Farahi et al., 2017). However, if the foundation is part of a structure with large footprint, then the rainwater will penetrate from one side of the building and thus the lateral flow of the water will also affect the degree of saturation of the soil in the influence depth of the foundation. In that situation, the two-dimensional form of the Richards equation must be used.

Since the pressure head is considered as the primary variable to be determined from the Richards equation in this study, the two other variables in Richards equation, θ and K, must be expressed as functions of ψ. The unsaturated hydraulic conductivity is expressed as $K = K_{sat}.K_r$, where K_{sat} is the hydraulic conductivity of the soil at fully saturated condition, and K_r is the relative hydraulic conductivity of the soil at partially saturated condition. Both θ and K_r are then expressed as functions of ψ using the SWCC for the soil. Among the many SWCCs and corresponding relative hydraulic conductivity functions available in the literature, the equations proposed by van Genuchten (1980) were used in this study. The mathematical formulations of the van Genuchten SWCC and the corresponding K_r functions are given in Eqs. (12) and (13), respectively.

$$\theta(\psi) = \theta_r + \frac{(\theta_s - \theta_r)}{[1 + (\alpha\psi)^n]^{(1-1/n)}} \tag{12}$$

$$K_r(\psi) = \frac{\{1 - (\alpha\psi)^{n-1}[1 + (\alpha\psi)^n]^{-(1-1/n)}\}^2}{[1 + (\alpha\psi)^n]^{(1-1/n)/2}} \tag{13}$$

where α and n are SWCC fitting parameters, θ_s is saturated water content, and θ_r is residual water content. Among the many numerical approaches used to solve the Richards equation (van Genuchten, 1982; Feddes et al., 1988; Celia et al., 1990; Warrick, 1991; Zaidel and Russo, 1992; Baker, 1995; Pan et al., 1996; Romano et al., 1998; Van Dam and Feddes, 2000), the Finite Volume Method (FVM) was used in this study. The spatial and temporal discretization and the key steps of the solution procedure are given in the following sections.

3.1. Numerical solution procedure

To solve the Richards equation, first, the equation needs to be written in term of the pressure head for one-dimensional vertical infiltration. Thus, $\frac{\partial\theta}{\partial t}$ is expressed as $\frac{\partial\theta}{\partial\psi}.\frac{\partial\psi}{\partial t} = C\frac{\partial\psi}{\partial t}$ and substituted in Eq. (11).

$$C\frac{\partial\psi}{\partial t} - \frac{\partial}{\partial z}\left(K\frac{\partial\psi}{\partial z} + K\right) = 0 \tag{14}$$

where C is the specific moisture capacity ($= \frac{\partial\theta}{\partial\psi}$). Then, the Eq. (14) is integrated with respect to the time (t) and depth (z) as follow.

$$\int_{i-1/2}^{i+1/2}\int_{t}^{t+\Delta t} C\frac{\partial\psi}{\partial t}dtdz - \int_{t}^{t+\Delta t}\int_{i-1/2}^{i+1/2}\frac{\partial}{\partial z}\left(K\frac{\partial\psi}{\partial z} + K\right)dzdt = 0 \tag{15}$$

where i is the node number (start from ground surface) and Δt is the time interval. The left-hand side of the integration is rewritten in a discretized form, which is expressed in Eq. (16).

$$\int_{i-1/2}^{i+1/2}\int_{t}^{t+\Delta t} C\frac{\partial\psi}{\partial t}dtdz = \int_{i-1/2}^{i+1/2} C(\psi^{t+\Delta t} - \psi^t)dz = C_i^{t+\Delta t}(\psi_i^{t+\Delta t} - \psi_i^t)\Delta z \tag{16}$$

The right-hand side is first solved for spatial variation, as shown in Eq. (17), and then, the integration is discretized into the temporal form, as shown in Eq. (18).

$$\int_{t}^{t+\Delta t}\int_{i-1/2}^{i+1/2}\frac{\partial}{\partial z}\left(K\frac{\partial\psi}{\partial z} + K\right)dzdt = \int_{t}^{t+\Delta t}\left[\left(K\frac{\partial\psi}{\partial z} + K\right)_{i+1/2} - \left(K\frac{\partial\psi}{\partial z} + K\right)_{i-1/2}\right]dt \tag{17}$$

$$C_i^{t+\Delta t}(\psi_i^{t+\Delta t} - \psi_i^t)\Delta z = \left[\left(K_{i+1/2}^{t+\Delta t}\frac{\psi_{i+1}^{t+\Delta t} - \psi_i^{t+\Delta t}}{\Delta z} + K_{i+1/2}^{t+\Delta t}\right) - \left(K_{i-1/2}^{t+\Delta t}\frac{\psi_i^{t+\Delta t} - \psi_{i-1}^{t+\Delta t}}{\Delta z} + K_{i-1/2}^{t+\Delta t}\right)\right]\Delta t \tag{18}$$

Considering m as the iteration level and pressure head at iteration $m + 1$ as the unknown value and Δz as the depth interval, the complete

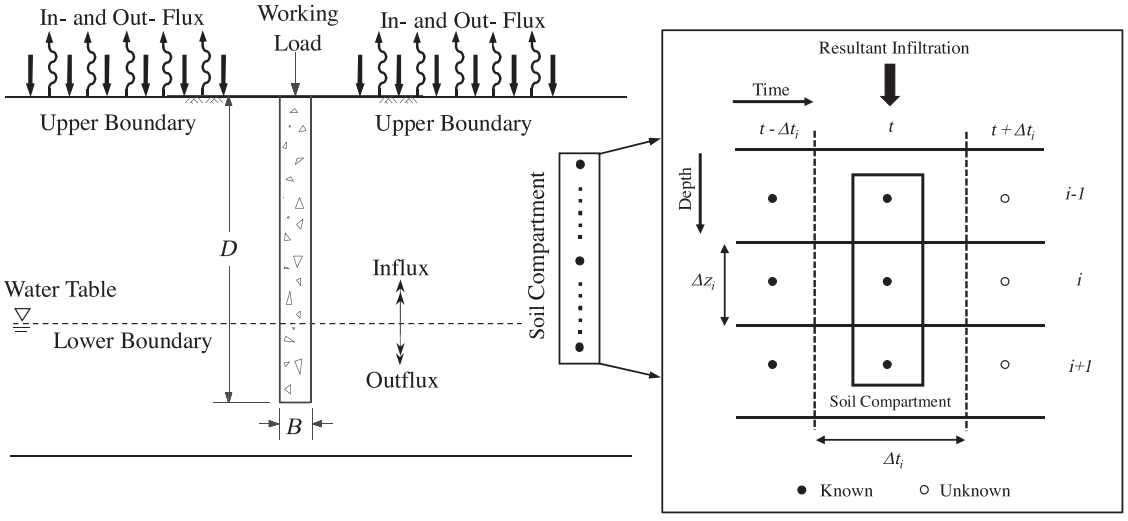

Fig. 2. Schematic of the proposed procedure for solving Richards equation (Mahmoudabadi and Ravichandran, 2019).

spatial and temporal form of Richards equation is expressed in Eq. (19).

$$C_i^{t+\Delta t,m}(\psi_i^{t+\Delta t,m+1}-\psi_i^{t})\Delta z= \left[\left(K_{i+1/2}^{t+\Delta t}\frac{\psi_{i+1}^{t+\Delta t,m+1}-\psi_i^{t+\Delta t,m+1}}{\Delta z}+K_{i+1/2}^{t+\Delta t}\right) -\left(K_{i-1/2}^{t+\Delta t}\frac{\psi_i^{t+\Delta t,m+1}-\psi_{i-1}^{t+\Delta t,m+1}}{\Delta z}+K_{i-1/2}^{t+\Delta t}\right)\right]\Delta t \quad (19)$$

Finally, dividing the Eq. (19) by Δz and rearranging the formulation, the final form of the Richards equation is written as follow (Eq. (20)).

$$C_i^{t+\Delta t,m}(\psi_i^{t+\Delta t,m+1}-\psi_i^{t}) =\left[\left(K_{i+1/2}^{t+\Delta t}\frac{\psi_{i+1}^{t+\Delta t,m+1}-\psi_i^{t+\Delta t,m+1}}{(\Delta z)^2}-K_{i-1/2}^{t+\Delta t}\frac{\psi_i^{t+\Delta t,m+1}-\psi_{i-1}^{t+\Delta t,m+1}}{(\Delta z)^2}\right) +\left(\frac{K_{i+1/2}^{t+\Delta t}-K_{i-1/2}^{t+\Delta t}}{\Delta z}\right)\right]\Delta t \quad (20)$$

3.2. Initial and boundary conditions

The one-dimensional numerical scheme of water infiltration into the soil profile is shown in Fig. 2 to illustrate the problem and the boundary conditions. The soil was assumed to be at the residual water content (initial condition) at the beginning of each simulation. The upper and lower boundaries for the simulation domain are the ground surface and the water table, respectively. In this study, both pressure head and flux were applied at the upper boundary depending upon the intensity of the resultant infiltration and the surface moisture capacity. In the case of ponding, that occurs when the infiltration rate is greater than the saturated hydraulic conductivity, the pressure head boundary condition is applied. On the contrary, when all water infiltrates into the soil, the flux boundary condition is applied. Since the water table location and resultant infiltration vary with climatic conditions for each specific location, appropriate values must be determined in a probabilistic manner considering historical rainfall, evapotranspiration, and water table data. The process of constructing the boundary conditions' probability distribution will be discussed in the design application section.

3.2.1. Resultant infiltration – upper boundary condition

The resultant infiltration, $F_{Resultnat\ Infiltration}$ as the upper boundary condition, is computed from subtraction of the influx from outflux climatic parameters for each specific site which is expressed in Eq. (21).

$$F_{Resultnat\ Infiltration} = Influx - Outflux = (F_{Rainfall}) - (F_{Evapotranspiration} + F_{Runoff}) \quad (21)$$

where $F_{Rainfall}$ is the historical rainfall intensity, $F_{Evapotranspiration}$ is the evapotranspiration intensity and F_{Runoff} is the surface runoff which is assumed to be zero in this study. One may consider topology and other site-specific parameters for calculating the resultant infiltration more accurately (Mahmoudabadi and Ravichandran, 2019).

3.2.1.1. Rainfall. The historical rainfall data were obtained from the National Climatic Data Center (NCDC) which records daily rainfall values. In this study, the annual maximum series were used and constructed by extracting the highest precipitation in each successive year over a given return period. Then, the maximum annual rainfall was tabulated for the same return period to determine the site-specific probability distribution of resultant infiltration.

3.2.1.2. Evapotranspiration. Land surface evaporation plus plant transpiration, evapotranspiration, is another climatic parameter which has a direct influence on the resultant infiltration and subsequently on the degree of saturation and matric suction of the subsurface area. This parameter is dependent on the other environmental factors such as temperature, daylight time, and saturated vapor density and can be simply computed based on the Hamon (1961) method in terms of Potential Evapotranspiration (*PET*) (Eq. (22)).

$$PET = 0.1651 \times L_d \times RHOSAT \times KPEC \quad (22)$$

where L_d is daytime length; T is the average air temperature; *KPEC* is a calibration coefficient equal to 1, and *RHOSAT* is saturated vapor density at a mean temperature calculated using Eq. (23).

$$RHOSAT = 216.7\frac{ESAT}{(T+273.2)} \quad (23)$$

where *ESAT* is the saturated vapor pressure and is calculated using the Eq. (24).

$$ESAT = 6.108\, e^{\frac{(17.27T)}{(T+237.3)}} \quad (24)$$

Using Hamon method, the daily potential evapotranspiration for the same return period, which was used for the rainfall data, is calculated based on the temperature values which were obtained from the National Oceanic and Atmospheric Administration (NOAA) of NCDC.

The key steps for computing the upper boundary condition are: (1) extract the site-specific historical rainfall data and temperature from NCDC, (2) calculate the site-specific resultant infiltration considering the historical rainfall, evapotranspiration, and surface runoff, (3) find the best-fitted probability distribution function for the site-specific resultant infiltration data, and (4) generate random number based on the distribution function to apply as the upper boundary condition through Monte Carlo simulation for each analysis. The detail of this process is described in the sample application section for the two study area considered in this study.

3.2.2. Water table - lower boundary condition

The water table, the lower boundary condition for solving the Richards equation, is another climatic parameter that affects the matric suction and degree of saturation of the soil along the shaft skin and tip. The required data was taken from the U.S. Geological Survey (USGS, 2016) for the same return period selected for the rainfall data. It should be noted that the lower boundary condition is applied as the head pressure. Similar to the resultant infiltration, the key steps for computing the lower boundary condition are: (1) extract the site-specific historical water table data from USGS, (2) find the best-fitted probability distribution function for the site-specific historical water table data, and (3) generate random number based on the distribution function to apply as the lower boundary condition through Monte Carlo simulation for each analysis. The detail of this process is described in the sample application section for the two study area considered in this study.

3.3. Model verification

The key to compute the spatial and temporal variation of degree of saturation in the soil for a given hydrological event is to accurately implement the Richards equation. Therefore, the accuracy of the model implementation must be validated against either the experimental results or the other models that are verified. In this study, the generalized solution developed by Celia et al. (1990) was used to verify the numerical implementation of the Richards equation. The comparison of the computed results and that computed by Celia et al. (1990) are shown in Fig. 3.

From the Fig. 3, it is clear that the implementation of the Richards equation is accurate and the model is ready for computing the spatial and temporal variation of degree of saturation during any hydrological/climatic events.

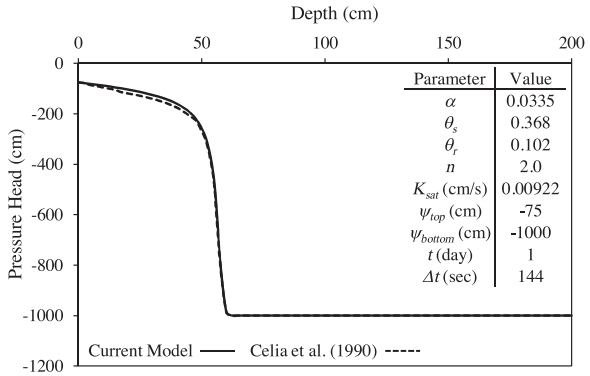

Fig. 3. Verification of numerical solution scheme.

4. Site-specific design application

The application of the proposed procedure requires the computation of temporal and spatial variation of matric suction and degree of saturation within the zone of influence. Because the skin resistance varies along the length of the shaft due to the spatial variation in degree of saturation, to accurately calculate the effect of hydrological/climatic parameters, the shaft needs to be divided into a number of segments along its length. The random variables associated with the climatic data are considered as the boundary conditions that change with return period and is discussed in details in the resultant infiltration and water table distribution section. Since these variables have time-independent uncertainty for each specific site, the probability analysis is required to adjust the design process. In another word, if the highest historical resultant infiltration rate and lowest water table depth are considered as the worst-case scenario of boundary conditions, the probability of occurrence of these events simultaneously is significantly low during the lifetime of structure. Considering this condition as one of the design cases can lead to an overdesign result. Thus, the design procedure

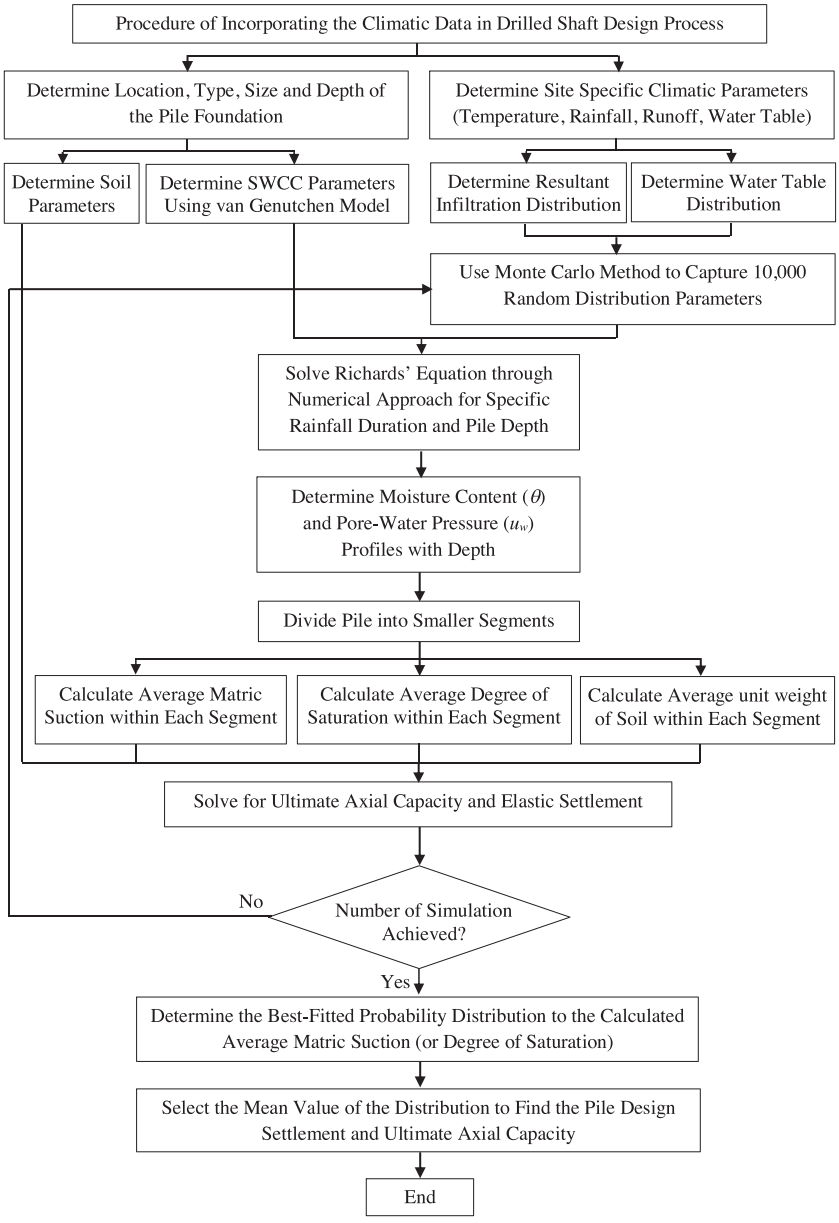

Fig. 4. Flowchart of proposed procedure for incorporating the hydrological data in geotechnical design of drilled shaft.

should be carried out through a probabilistic manner to consider all the occurrence possibilities of climate events. This way of analysis will lead to a more realistic design approach based on the Probability Density Function (PDF) of the climate-related geotechnical parameters for the drilled shaft.

To perform the probabilistic analysis, first, the probability distributions of historical resultant infiltration rate and water table depth were used by Monte Carlo simulation method to generate a set of random input variables. These input variables were considered as the boundary conditions in this study. Then, the solution to Richards equation was used to compute the temporal and spatial variation of soil degree of saturation and matric suction along the shaft skin. Afterward, the ultimate axial capacity and elastic settlement of each drilled shaft were calculated using the average degree of saturation and matric suction. This process was repeated for all the generated input variables. Finally, the mean of the best-fitted probability distribution to the average matric suction is selected to find the design axial capacity and settlement of drilled shaft for study sites. The mean value selected in this study is a good representative of dominant matric suction and degree of saturation occurred for each site considering historical rainfall (maximum recorded rainfall intensity for each year). In other words, the degree of saturation obtained from the proposed analysis can be considered as the maximum historical site-specific degree of saturation over the design life of the foundation. Since the actual site-specific matric suction and degree of saturation are the key parameters that must be accurately determined for the design, the mean value can be considered as a good estimate of the site-specific degree of saturation for practical applications instead of assuming fully saturated condition. It should be noted that the inherent randomness of shear strength parameters of the soil can also be incorporated into the analysis, but for the comparison between the saturated and partially saturated conditions, the shear strength variables were kept as constants throughout the analysis except the soil unit weight. The soil unit weight changes with varying degrees of saturation computed along the shaft skin for each simulation. It is worth mentioning that, although there may be a strong correlation between the historical rainfall and water table when the rainfall infiltrates into the ground completely, the rainfall and water table depth were considered as independent variables in the probabilistic analysis. This is because there is no realistic correlation coefficient available in the literature that considers the key factors such as rainfall intensity and duration, evapotranspiration, human activities (i.e. water pumping and water usage) and site characteristics (i.e. topography and urbanization) in the correlation. Therefore, these two events/boundary conditions (rainfall and water table depth) are considered as two independent variables in this study. The flowchart of the procedure employed in this study is presented in Fig. 4.

Table 2
Basic geotechnical parameters for Salt Lake City, UT and Riverside, CA sites.

Parameter	Salt Lake City, UT	Riverside, CA
Dry unit weight, γ_d (kN/m^3)	16.40	18.10
Void ratio, e_s	0.585	0.436
Effective friction angle, ϕ' (deg)	32	30
Effective adhesion, c'_a(kPa)	7	5
Plasticity Index, I_p	11	7

4.1. Study sites

Two sites in the USA were selected in this study to show the effects of climatic parameters on the ultimate axial capacity and elastic settlement of drill shafts. The first site is located in Salt Lake City, UT. The Salt Lake City site was selected due to its semi-arid climate and availability of van Genuchten SWCC parameters, in addition to the conventional geotechnical engineering parameters for the silty-clayey sandy (SC) soil type found in this region. The SWCC parameters were obtained from the report by Zhang (2010). The soil strength parameters of the site were obtained from a geotechnical report by GSH Geotechnical Inc. (2013) and Web Soil Survey developed by the United States Department of Agriculture (USDA, 2016). A location in Riverside, CA, was selected as the second site which mostly contains the silty sand (SM). For this site, the soil strength parameters were obtained from a geotechnical report provided by Converse Consultants (2016) and Web Soil Survey developed by the United States Department of Agriculture (USDA, 2016). The SWCC parameters for the Riverside location were obtained from the report by Zhang (2010). The specified van Genuchten SWCC parameters model for these two locations are presented in Fig. 5. In addition, the basic strength and other geotechnical parameters for both locations are listed in Table 2.

4.2. Probability distribution of boundary conditions

As is discussed in previous sections, the boundary conditions, resultant infiltration as an upper boundary condition and water table as a lower boundary condition, are highly relied on the climatic parameters which change with various return periods. Thus, these boundary conditions need to be represented separately by a probability distribution instead of a deterministic value. The return period selected for this study was 117 years for both study locations (NCDC, 2016). The process of producing the boundary conditions' distribution is explained in detail below.

4.2.1. Constructing probability distribution

To determine the best fitting distribution for the resultant

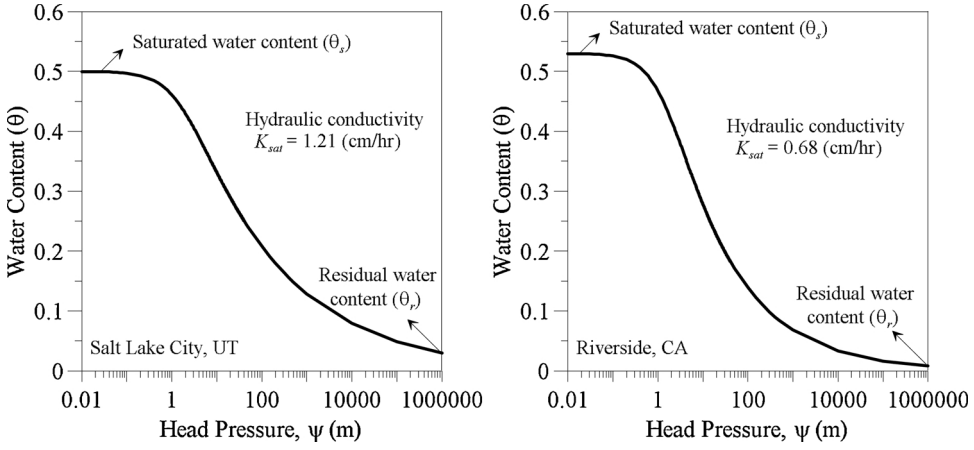

Fig. 5. van Genuchten SWCC for Salt Lake City and Riverside sites.

infiltration and water table data, the probability paper plotting technique was used. Type I Extreme Largest (Gumbel distribution), the Type II Extreme Largest (Frechet distribution), and the Type III Extreme Largest (Weibull distribution) were checked for the best fit, and the Gumbel distribution was deemed to be the best regression based on the R-squared test (R^2-value). The Gumbel probability paper distribution parameters, mode (μ_n) and standard deviation (β_n), can be determined using Eq. (25).

$$x_v = y_v\beta_n + \mu_n = -\ln\left(-\ln\left(\frac{v}{r+1}\right)\right)\beta_n + \mu_n \quad (25)$$

where v is the data index (arranged in increasing order), x_v is the annual maximum historical rainfall or water table data, y_v is the linearized form of the cumulative density function of Gumbel distribution, and r is the number of data points. The probability plots of the resultant infiltration and water table depth based on the Gumbel distribution are shown in Figs. 6 and 7, respectively, for both study sites.

4.3. Climatic loads

The climatic load is applied in the proposed framework through the upper boundary (historical rainfall and evapotranspiration) and lower boundary (groundwater table depth) conditions as well as the duration of the climate event. As described before, the boundary condition for each simulation is predicted through the probability distribution function for each location using Eq. (25). In addition, the duration of the climate events was assumed to be 1, 3 and 5 days in this study based on the examination of the historical rainfall data.

4.4. Initial design and design parameters

Drilled shaft with width, B = 0.9, 1.2 and 1.5 m and length, D = 12, 15 and 18 m were considered in this study to investigate the influence of the climate parameters on the size of the foundation. The applied working load for each drilled shaft was calculated based on the fully saturated soil condition and a factor of safety 3.0 was assumed for both skin and tip resistances.

4.5. Computational platform

For considering the historical rainfall and water table depth in a probabilistic manner, the Richards equation must be solved around 10,000 times by randomly selecting the rainfall intensity and water table depth and the skin resistance, tip resistance, and settlement must be calculated for each simulation. To automate such repeated calculations, a MATLAB code was developed, parallelized, and installed on the Clemson University's High-Performance Computing (HPC) System called Palmetto Cluster. A simulation that took almost a month on a single processor PC was completed within a week with just four nodes on the Palmetto Cluster.

5. Results and discussion

5.1. 3-Day rainfall analyses

5.1.1. Average matric suction and degree of saturation

To show the impact of rainfall and water table depth on the bearing capacity and settlement of drill shaft, a 3-day continuous rainfall was considered. The intensity of the rainfall and the water table depth vary with time and therefore considered in a probabilistic manner to compute an average head pressure and the corresponding degree of saturation within the influence zone of the drilled shaft. For that, 10,000 scenarios of rainfall intensity and water table depth were randomly selected using the Monte Carlo simulation technique based on the probability distribution of the resultant infiltration and water table depth for each site. The variation of average matric suction and the corresponding degree of saturation were computed based on the 10,000 simulations and plotted as shown in Fig. 8 for both sites. The average degree of saturation at the Riverside, CA site varies between 54% and 96% while this range is in between 81% and 97% for the Salt Lake City, UT site. This difference may be attributed to the difference in the soil type, intensity of rainfall and water table depth.

5.1.2. Variation of elastic settlement

Changing in matric suction and degree of saturation, due to the site-specific climatic parameters, affect the soil stiffness which directly influences the elastic settlement of the drilled shaft. As is presented in Fig. 9, increasing the matric suction has a considerable impact on reducing the drilled shaft elastic settlement for both sites. Each line in the figures represents the 10,000 analysis considering the random resultant infiltration intensity and water table depth as the upper and lower boundary conditions, respectively which were already discussed. For each analysis, the spatial variation of the degree of saturation and matric suction beneath the ground surface was determined. Then, the average degree of saturation and matric suction were calculated along the shaft skin and were used to compute the soil stiffness and subsequently the elastic settlement. Based on the results, the elastic settlement of the drilled shaft in Riverside shows the greater elastic settlement compared to that in Salt Lake City for the same size of foundation. It was found that each case in Riverside site experienced a significant decrease in the elastic settlement within a range of 78–102 kPa matric suction which is caused by the existence of water table at the tip level

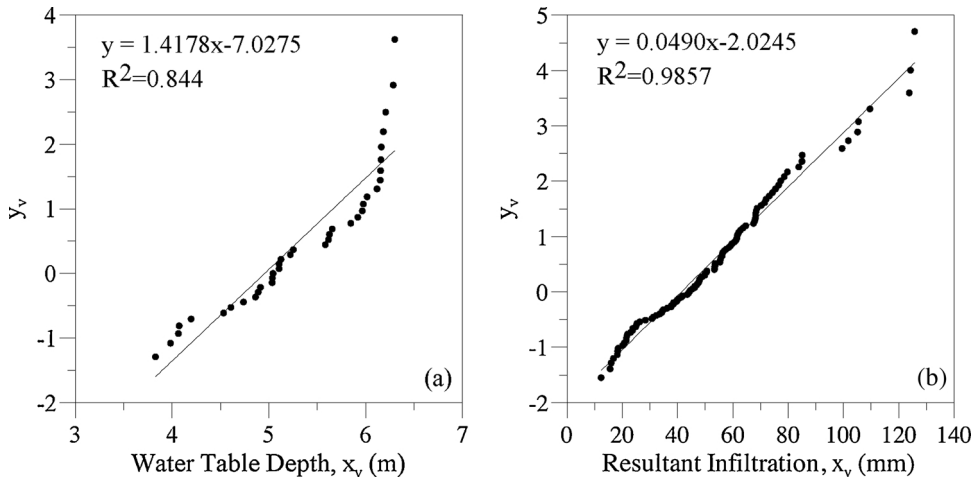

Fig. 6. Gumbel distribution for water table depth and resultant infiltration for Salt Lake City.

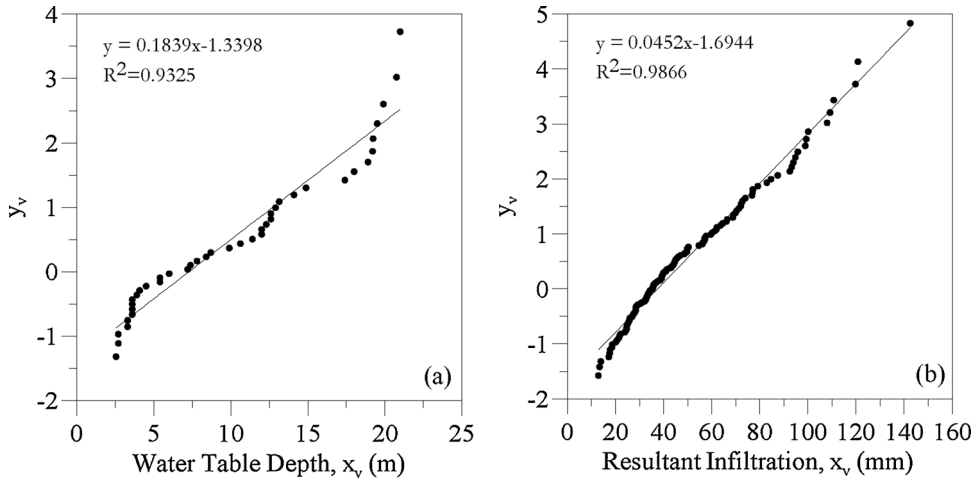

Fig. 7. Gumbel distribution for water table depth and resultant infiltration for Riverside.

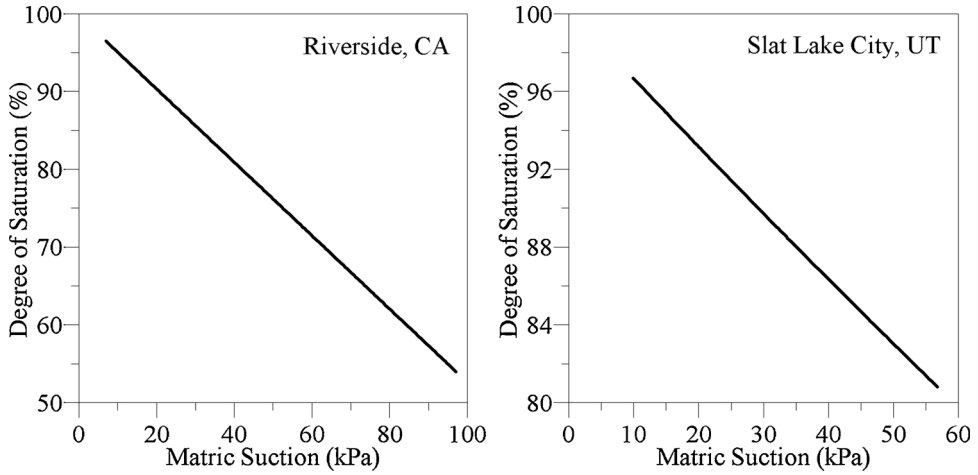

Fig. 8. Predicted variation of average matric suction with degrees of saturation (Left: Riverside, CA and Right: Salt Lake City, UT).

for different simulations. Afterwards, the settlement reduces gradually. This significant decrease in the total elastic settlement is mainly caused by the shaft tip settlement in which the groundwater level reduction increased the soil stiffness. It should be noted that this effect is not captured in the Salt Lake City site because of shallow groundwater depth in this area where the water level is placed well-above the shaft tip level over the selected period.

5.1.3. Variation of ultimate axial capacity

Regarding the shaft skin and tip resistance, the results of the proposed method depict an increasing trend for each shaft size due to an increase of matric suction in both locations (Figs. 10 and 11). However, as is observed from elastic settlement results, the effect of water table also has a considerable effect on increasing the tip resistance in the same suction range which is already discussed and highlighted in

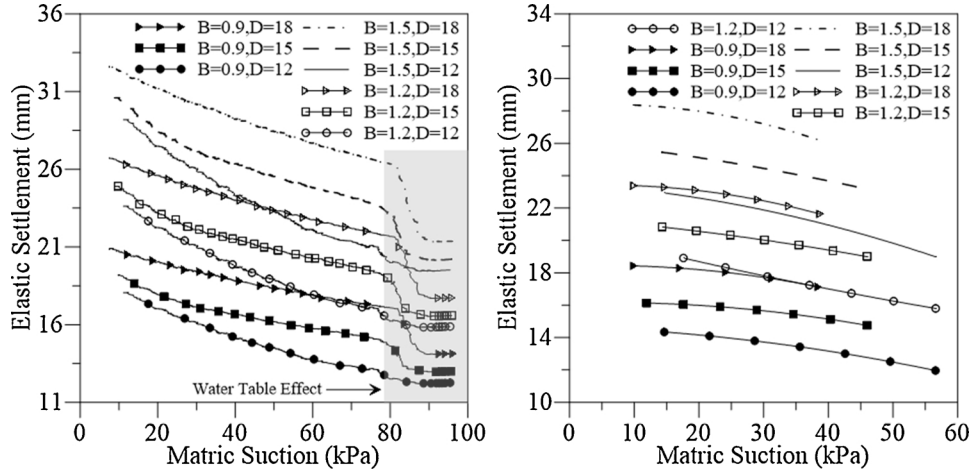

Fig. 9. Predicted variation of elastic settlement with matric suction after 3-day continuous rainfall (Left: Riverside, CA and Right: Salt Lake City, UT).

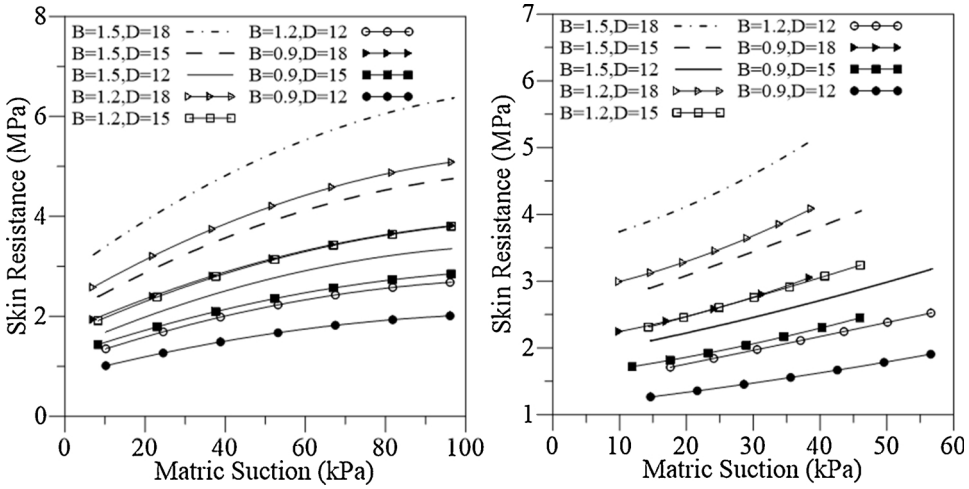

Fig. 10. Predicted variation of skin resistance with matric suction after 3-day continuous rainfall (Left: Riverside, CA and Right: Salt Lake City, UT).

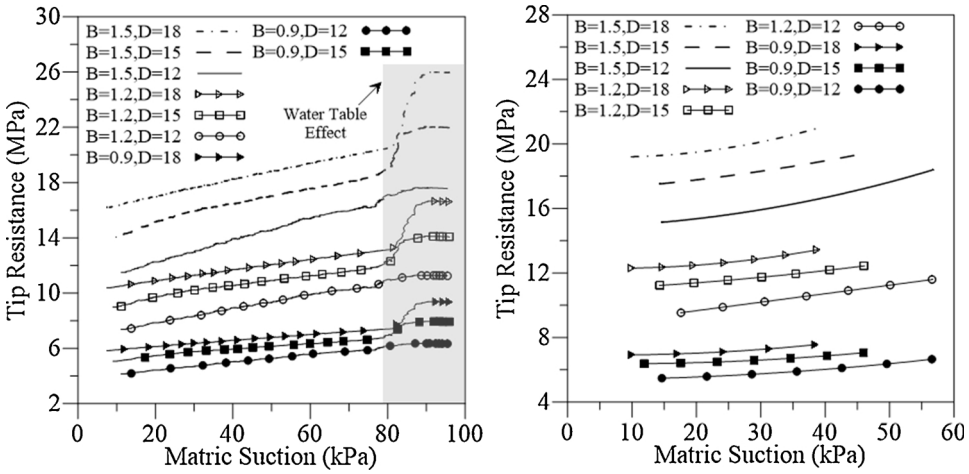

Fig. 11. Predicted variation of tip resistance with matric suction after 3-day continuous rainfall (Left: Riverside, CA and Right: Salt Lake City, UT).

Fig. 11. Also, it can be seen that the shaft tip shows greater resistance in comparison with the skin for each shaft size.

The ultimate axial capacity of different drilled shafts based on the proposed method is presented in Fig. 12 for both sites. As is shown in the figure, the increasing trend of the axial capacity is similar to the trend of shaft tip resistance in which the shaft depth controls the ultimate design values. Based on the results, it can be concluded that the soil matric suction, which highly depends on the degree of saturation of the soil profile and site-specific climatic loads, has a significant effect on the ultimate axial capacity of the drilled shaft and subsequently on its design procedure.

5.1.4. *Effect of drilled shaft size*

According to the results, the size of the shafts have a significant

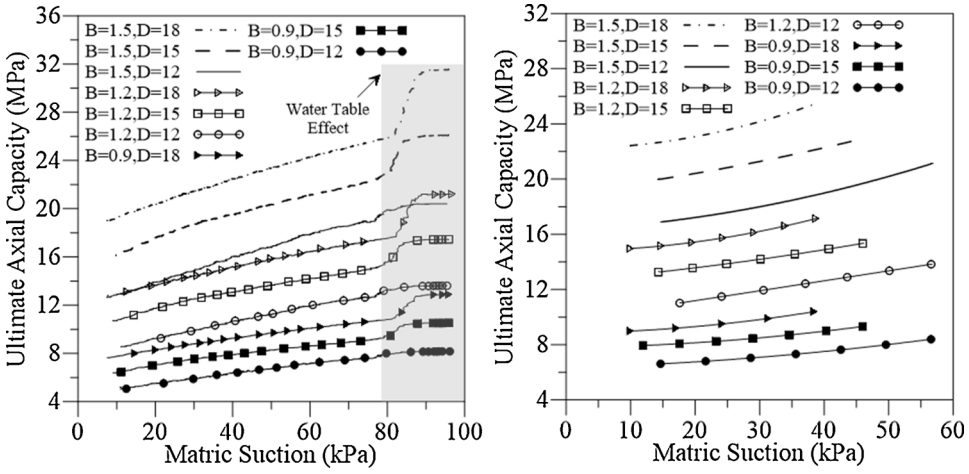

Fig. 12. Predicted variation of ultimate axial capacity with matric suction after 3-day continuous rainfall (Left: Riverside, CA and Right: Salt Lake City, UT).

impact on the elastic settlement and ultimate axial capacity. In case of the elastic settlement, it can be seen that the width of the shaft has a greater impact compared to the depth factor. On the other hand, for the ultimate axial capacity, it is found that the shaft depth factor has more impact on the skin resistance in comparison with the width factor, while this is vice-versa for the tip resistance.

5.1.5. Foundation design values determination and comparison with deterministic approach

To assess the impact of the climatic parameters in the design of drilled shaft, a comparison between the proposed method and the deterministic approach in which the soil is assumed fully saturated, is required. To this end, first, the design settlement and axial capacity should be determined based on the proposed method considering all the possible scenarios of climatic parameters for each study site. The hydro-climatic parameters, as is discussed before, alter the settlement and axial capacity of the drilled shaft through changing the matric suction and degree of saturation of the underlying soil. Thus, a simple way to determine the design values is to find the most probable average matric suction (or degree of saturation) of the site considering all the scenarios. Since these scenarios are selected based on the probability distribution of boundary conditions (resultant infiltration and water table depth) for each location, it can be concluded that the calculated average matric suction covers all the possible scenarios of climatic parameters for designing the drilled shaft reasonably well. Therefore, the mean value of the best-fitted probability distribution to the matric suction is deemed to be the best-selected input value for computing the design settlement and axial capacity. The same distributions, which were used for finding the best-fitted distribution of boundary conditions, are again considered here. Weibull distribution was deemed to be the best regression to the average matric suction based on Kolmogorov-Smirnov test (p-value) for both locations. As is shown in Fig. 13, the mean value of matric suction for Salt Lake City and Riverside are 23.4 kPa and 49.8 kPa, respectively. Using the mean values, the ultimate axial capacity and elastic settlement of each shaft can be easily found from Figs. 9 and 12 as the design values. It should be noted that the average degree of saturation can also be found for each site using Fig. 8.

For the deterministic design approach, the elastic settlement and ultimate axial capacity including skin and tip resistance of each case study were computed using Das' and Kulhawy's (Kulhawy and Mayne, 1990; Das, 2010) general equations for both sites. The design values of each case study using the presented method are determined based on the mean value of average matric suction for each study location. As are shown in Tables 3 and 4, the ultimate axial capacity of each drilled shaft increases by as much as 40% of the conventional method in Salt Lake City, while this is utmost 56% for Riverside. In case of the settlement criteria, the total elastic settlement of each drilled shaft decreases by utmost 34% and 30% at Salt Lake City and Riverside, respectively. It can be concluded from this comparison that the effect of matric suction in design parameters of the drilled shaft depends on the SWCC and also inherent soil characteristics of a site location, which is highly relied on the climatic parameters and also water table level.

5.2. Parametric study-impact of rainfall duration

In this section, different time durations (1, 3 and 5 days) are selected to assess the design parameters of a drilled shaft with the width of 0.9 m and depth of 12 m. The analysis is performed considering the same boundary conditions which were used for the previous set of analysis. Fig. 14 shows the spatial variation of the degree of saturation with different time duration of resultant infiltration. As is discussed before, the inherent soil characteristics and SWCC of each site has a direct effect on the water infiltration process and subsequently the water penetration depth. It can be seen from the figure that when the time duration increase from 1 to 5 days, water penetrates utmost 1.0 m into the subsurface area for Riverside, while this depth is almost 3.2 m for Salt Lake City, although the location of the water table presents a tendency to remain unchanged during the analysis for all simulations. The reason is that the final depth of infiltrated water is always placed above the water table level throughout all simulations.

Based on the finding from the results, various time durations change the depth of infiltrated water and subsequently vary the matric suction and soil stiffness of subsurface specifically the area close to the upper shaft segments. This change affects the shaft skin resistance and ultimately the axial capacity and elastic settlement of drilled shaft.

As is presented in Fig. 15, the total elastic settlement of the drilled shaft is obtained from the proposed method considering different rainfall durations of resultant infiltration. It is clear that since water does not penetrate too deep into the soil for the Riverside site, the average matric suction and degree of saturation of shaft segments do not experience too much change over different periods which lead to small change in elastic settlement for the drilled shaft. However, the elastic settlement of Salt Lake City shows noticeable changes due to different durations for lower matric suction values.

The skin resistance of the drilled shaft with various time durations is shown in Fig. 16 for both locations. Similar to the results of elastic settlement for Riverside, the variation of skin resistance does not present any discrepancy, while there is a small change in shaft skin resistance in the Salt Lake City region for different time durations, although at higher matric suction the results are closer to each other.

Finally, the ultimate axial capacity of the drilled shaft is calculated based on the proposed method considering different time periods and presented in Fig. 17. Like previous results for the Riverside region, the time parameter slightly affects the ultimate axial capacity which is

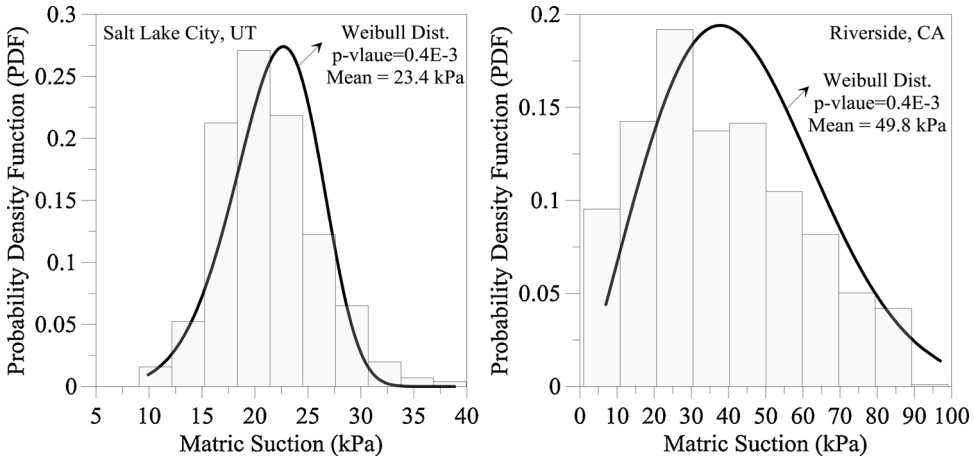

Fig. 13. Best-fitted distribution of average matric suction within the influence zone of the foundation (Left: Salt Lake City, UT and Right: Riverside, CA).

Table 3
Comparison of drilled shaft design parameters considering proposed method and fully saturated condition in Riverside.

Width (B) (m)	Depth (D) (m)	Fully Saturated Condition				Difference [(Unsat-Sat)/Sat)*100] (%)			
		Q^{Skin} (kPa)	Q^{Tip} (kPa)	Q_{Ult} (kPa)	S_e (mm)	Q^{Skin}	Q^{Tip}	Q_{Ult}	S_e
1.50	18.0	2659.78	15076.75	17297.89	34.82	+95.49	+25.43	+35.77	−18.70
1.50	15.0	1905.97	12556.05	14096.49	33.96	+101.61	+35.17	+43.99	−24.59
1.50	12.0	1276.37	10035.56	11019.51	33.28	+110.50	+43.96	+51.72	−29.48
1.20	18.0	2127.82	9655.28	11502.38	28.49	+95.49	+25.53	+38.06	−18.32
1.20	15.0	1524.78	8041.96	9332.79	27.60	+101.61	+35.31	+45.98	−24.28
1.20	12.0	1021.10	6428.70	7262.64	26.90	+110.50	+44.14	+53.52	−29.26
0.90	18.0	1595.87	5434.60	6872.56	22.21	+95.49	+25.64	+41.47	−17.74
0.90	15.0	1143.58	4527.08	5539.07	21.27	+101.61	+35.44	+48.95	−23.74
0.90	12.0	765.82	3619.57	4280.12	20.54	+110.51	+44.32	+56.22	−28.87

Table 4
Comparison of drilled shaft design parameters considering proposed method and fully saturated condition in Salt Lake City.

Width (B) (m)	Depth (D) (m)	Fully Saturated Condition				Difference [(Unsat-Sat)/Sat)*100] (%)			
		Q^{Skin} (kPa)	Q^{Tip} (kPa)	Q_{Ult} (kPa)	S_e (mm)	Q^{Skin}	Q^{Tip}	Q_{Ult}	S_e
1.50	18.0	2654.79	17321.57	19537.72	35.09	+61.37	+13.64	+19.93	−20.97
1.50	15.0	1926.07	14581.35	16141.89	34.15	+69.97	+24.42	+29.83	−27.82
1.50	12.0	1311.85	11658.56	12677.99	33.38	+75.66	+36.20	+40.44	−34.33
1.20	18.0	2123.83	11090.18	12933.29	28.78	+61.37	+13.71	+21.39	−20.54
1.20	15.0	1540.86	9336.40	10643.32	27.81	+69.97	+24.52	+31.07	−27.40
1.20	12.0	1049.48	7465.65	8327.98	27.01	+75.66	+36.36	+41.46	−33.99
0.90	18.0	1592.87	6240.74	7675.70	22.51	+61.38	+13.77	+23.48	−19.86
0.90	15.0	1155.64	5254.23	6278.28	21.49	+69.97	+24.62	+32.95	−26.66
0.90	12.0	787.11	4201.88	4883.72	20.66	+75.66	+36.52	+42.97	−33.45

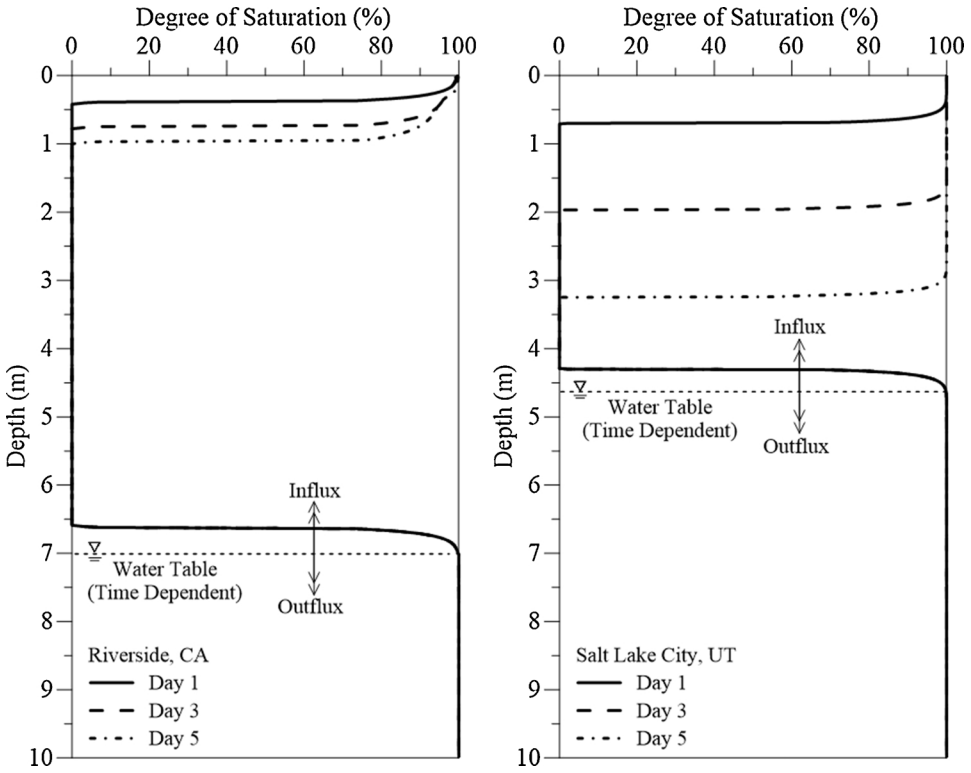

Fig. 14. Degree of saturation profile at the end of each rainfall duration.

caused by the fine-grained soil existing in that region. However, the influence of water infiltration period is noticeably observed in Salt Lake City in which the differences are higher at the lower matric suction, while they get close to each other at greater matric suction. Also, it is cleared that for longer time periods, the results of the ultimate axial capacity decrease because of increasing the degree of saturation of soil profile which leads the subsurface to become close to the fully saturated condition.

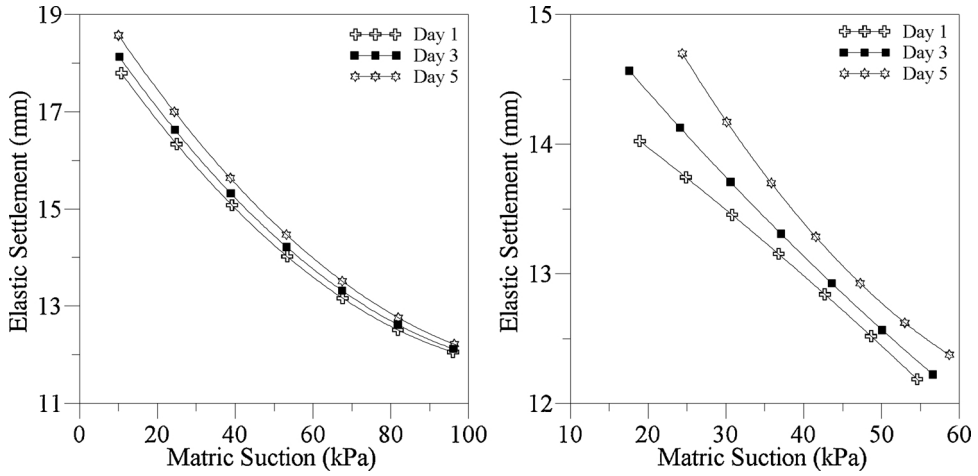

Fig. 15. Predicted variation of elastic settlement with matric suction for different rainfall duration (Left: Riverside, CA and Right: Salt Lake City, UT).

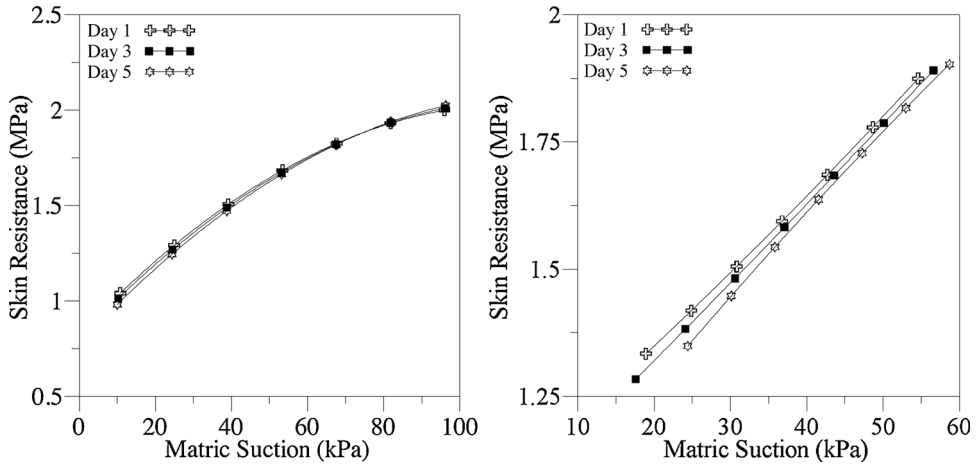

Fig. 16. Predicted variation of skin resistance with matric suction for different rainfall duration (Left: Riverside, CA and Right: Salt Lake City, UT).

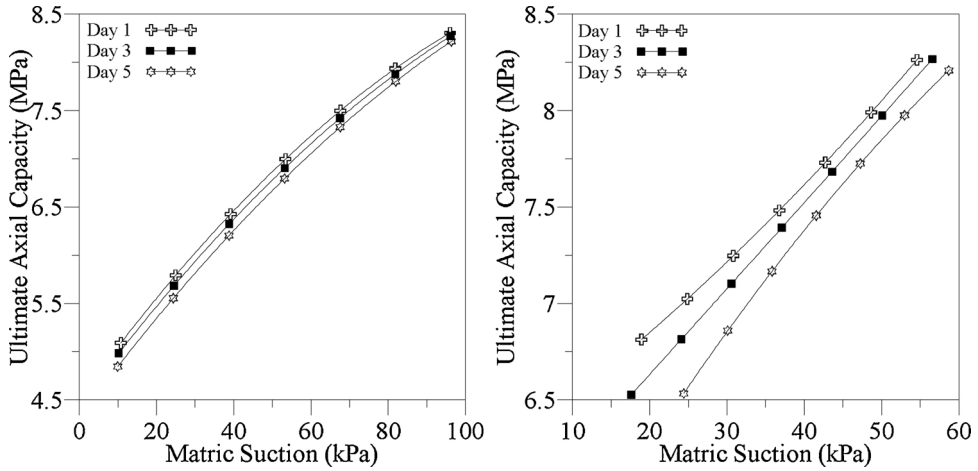

Fig. 17. Predicted variation of ultimate axial capacity with matric suction for different rainfall duration (Left: Riverside, CA and Right: Salt Lake City, UT).

6. Summary and conclusion

The coupled geotechnical-climatic scheme defined in this study was used to incorporate the climatic and subsurface data with the deterministic methods used in drilled shaft design. This novel method evaluates ultimate axial capacity and elastic settlement due to matric suction and degree of saturation of the soil along the shaft skin. The resultant infiltration of rainwater and evapotranspiration through initially partially saturated soil was modeled using the one-dimensional Richards equation considering both resultant infiltration rate and water table location as the upper and lower boundary conditions, respectively. To calculate the axial capacity and settlement of various drilled shafts, the average degree of saturation and matric suction along the shaft skin for each pile segment were computed by applying 10,000 random input values corresponding to the resultant infiltration and water table distributions using Monte Carlo simulation.

Two sample sites were selected in this study to show the variation of ultimate axial capacity and elastic settlement with matric suction; Riverside, CA and Salt Lake City, UT. After a three days continuous water infiltration and ignoring the effect of surface runoff, the degree of saturation in Riverside was between 54% and 96%, and between 97% and 80% in Salt Lake City. The significant difference in the ranges is caused by the existence of the fine-grained soil in the Riverside, CA site which decreases the soil porosity and makes it less permeable. It is also found that considering the matric suction in a drilled shaft design increases the ultimate axial capacity of a shaft by as much as 40% of the conventional method using fully saturated condition in Salt Lake City, while this is utmost 56% for Riverside. In case of the settlement criteria, the total elastic settlement of drilled shaft decreases by utmost 34% and 30% at Salt Lake City and Riverside, respectively. Also, the results show that the water table level had a noticeable impact on the design parameters of drilled shafts specifically in Riverside in which each case experience a significant decrease in the total settlement and increase in the ultimate axial capacity within a range of 78–102 kPa matric suction. This result is caused by the existence of the water table at the shaft tip level for different simulations. This significant change is mainly caused by the shaft tip in which the groundwater level reduction is increased the soil stiffness

However, the effect of the matric suction can be changed depending upon the depth of water infiltration into the soil. Thus, three rainfall durations (1, 3 and 5 days) are selected to assess the design parameters of a drilled shaft with the width of 0.9 m and depth of 12 m. As the results presented, the inherent soil characteristics of each site location have a direct effect on the water infiltration process and subsequently the depth at which water penetrates. When the time increases from 1 to 5 days, water penetrates utmost 1.0 m into the subsurface area for Riverside, while it goes deeper for Salt Lake City which was almost 3.2 m. Therefore, various time durations change the depth of infiltrated water and subsequently vary the matric suction and soil stiffness of subsurface specifically the area close to the upper shaft skin. This change affects the shaft skin resistance and ultimately the axial capacity and elastic settlement of drilled shaft. Because of greater water penetration in Salt Lake City, increasing the time duration of resultant infiltration leads to a decrease of ultimate axial capacity and raise of settlement in that region, while the design parameters of Riverside remain mostly unchanged due smaller depth on water penetration.

Funding

This research did not receive any specific grant from funding agencies in the public, commercial, or not-for-profit sectors.

References

Agarwal, K.G., Rana, M.K., 1987. Effect of ground water on settlement of footing in sand. In: Proc 9th Eur. Conf. on Soil Mechanics and Foundation Engineering. Dublin. pp. 751–754 2.

Baker, D.L., 1995. Darcian weighted interblock conductivity means for vertical unsaturated flow. Ground Water 33 (3), 385–390.

Borana, L., Yin, J.H., Singh, D.N., Shukla, S.K., 2015. A modified suction controlled direct shear device for testing unsaturated soil and steel plate interface. Mar. Georesour. Geotechnol. 33 (4), 289–298.

Borana, L., Yin, J.-H., Singh, D.N., Shukla, S.K., 2016. Interface behavior from suction-controlled direct shear test on completely decomposed granitic soil and steel surfaces. Int. J. Rock Mech. Min. Sci. https://doi.org/10.1061/(ASCE)GM.1943-5622.0000658.

Briaud, J.-L., 2013. Geotechnical Engineering: Unsaturated and Saturated Soils. Wiley, Chichester, U.K.

Celia, M.A., Bouloutas, E.T., Zarba, R.L., 1990. A general mass conservative numerical solution for the unsaturated flow equation. Water Resour. Res. 26, 1483–1496.

Converse Consultants, 2016. Revised Geotechnical Investigation Report. Redlands, CA. .

Costa, Y.D., Cintra, J.C., Zornberg, J.G., 2003. Influence of matric suction on the results of plate load tests performed on a lateritic soil deposit. Geotech. Test. J. 26 (2), 219–226.

Das, B.M., 2010. Principles of Foundation Engineering. Cengage Learning, Stamford, USA.

Douthitt, B., Houston, W., Houston, S., Walsh, K., 1998. Effect of wetting on pile friction. Proc. 2nd Int. Conf. on UNSAT 219–224.

Feddes, R.A., Kabat, P., Van Bakel, P.J.T., Bronswijk, J.J.B., Halbertsma, J., 1988. Modelling Soil Water Dynamics in the Unsaturated Zone-State of the Art. J. Hydrol. 100, 69–111.

Fredlund, D.G., Morgenstern, N.R., Widger, R.A., 1978. The shear strength of unsaturated soils. Can. Geotech. J. 15 (3), 313–321.

Fredlund, D.G., Rahardjo, H., Fredlund, M.D., 2012. Unsaturated Soil Mechanics in Engineering Practice. Wiley, Chichester, U.K.

Farahi, G., Khodashenas, S., Alizadeh, A., Ziaei, A., 2017. New Model for Simulating Hydraulic Performance of an Infiltration Trench with Finite-Volume One-Dimensional Richards' Equation. J. Irrig. Drain. Eng. 143 (8). https://doi.org/10.1061/(ASCE)IR.1943-4774.0001176.

Garven, E.A., Vanapalli, S.K., 2006. Evaluation of empirical procedures for predicting the shear strength of unsaturated soils. In: Proc., 4th Int. Conf. of Unsaturated Soil. UNSAT 2006. ASCE Geotechnical Special Publication 147, ASCE, Reston, Va., 2570–2581.

Georgiadis, K., Potts, D.M., Zdravkovic, L., 2003. The Influence of Partial Soil Saturation Pile Behavior. Gotechnique 53, 11–25.

GSH Geotechnical Inc, 2013. Report Supplemental Geotechnical Study Lots 1901 To 1907, Eaglepoint Estates Approximately 950 South Parkway Drive North Salt Lake, Utah. Salt Lake City, UT. .

Guan, G.S., Rahardjo, H., Choon, L.E., 2010. Shear strength equations for unsaturated soil under drying and wetting. J. Geotech. Geoenv. Eng. https://doi.org/10.1061/(ASCE)GT.1943-5606.0000261.

Hamon, W.R., 1961. Estimating potential evapotranspiration. J. Hydraul. Div. 87 (3), 107–120.

Khoury, C.N., Miller, G.A., Hatami, K., 2010. Unsaturated soil geotextile interface behavior. Geotext. Geomembr. 29, 613–624.

Kim, Y., Park, H., Jeong, S., 2017. Settlement behavior of shallow foundations in unsaturated soils under rainfall. Sustainability 9, 1417.

Kulhawy, F.H., Mayne, P.W., 1990. Manual on Estimating Soil Properties for Foundation Design. Report EL-6800, Electric Power Research Institute, Palo Alto, CA.

Kulhawy, F.H., 1991. Drilled Shaft foundations. In: Fang, H.Y. (Ed.), Foundation Engineering Handbook. Springer, Boston, MA.

Lee, I.-M., Sung, S.-G., Cho, G.-C., 2005. Effect of stress state on the unsaturated shear strength of a weathered granite. Can. Geotech. J. 42, 624–631.

Lu, N., Likos, W.J., 2004. Unsaturated Soil Mechanics. Wiley, Chichester, U.K.

Mahmoudabadi, V., Ravichandran, N., 2017. A coupled geotechnical-hydrological model for computing bearing capacity and settlement of shallow foundation. In: Proc. 2nd Pan-American Conference on Unsaturated Soils. Dallas, TX.

Mahmoudabadi, V., Ravichandran, N., 2019. A procedure for incorporating climatic and water table data in the geotechnical design of driven pile subjected to axial load. In: Proc. 8th International Conference on Case Histories in Geotechnical Engineering (Geo-Congress 2019). American Society of Civil Engineers (ASCE), Philadelphia, PA.

Moftakhari, H.R., AghaKouchak, A., Sanders, B.F., Matthew, R.A., 2017. Cumulative hazard: the case of nuisance flooding. Earth's Future 5 (2), 214–223.

National Climatic Data Center (NCDC), U.S Department of Commerce, 2016. NOAA Satellite and Information Service. National Environmental Satellite, Data, and Information Service. accessed December. http://www.ncdc.noaa.gov/oa/ncdc.html.

Oberg, A., Sallfors, G., 1997. Determination of shear strength parameters of unsaturated silts and sands based on water retention curve. Geotech. Test. J. 20, 40–48.

Oh, W.T., Vanapalli, S.K., Puppala, A.J., 2009. Semi-empirical model for the prediction of modulus of elasticity for unsaturated soils. Can. Geotech. J. 46 (8), 903–914.

Pan, L., Warrick, A.W., Wierenga, P.J., 1996. Finite elements methods for modelling water flow in variably saturated porous media: numerical oscillation and mass distributed schemes. Water Resour. Res. 32, 1883–1889.

Robinson, J.D., Vahedifard, F., AghaKouchak, A., 2017. Rainfall-triggered slope instabilities under a changing climate: comparative study using historical and projected precipitation extremes. Can. Geotech. J. 54 (1), 117–127.

Ravichandran, N., Mahmoudabadi, V., Shrestha, S., 2017. Analysis of the bearing capacity of shallow foundation in unsaturated soil using Monte-Carlo simulation. Int. J. Geosci. 8 (10), 1231–1250.

Richards, L.A., 1931. Capillary conduction of liquids through porous mediums. Physics 1 (5), 318–333.

Rojas, J.C., Salinas, L.M., Seja, C., 2007. Plate-load tests on an unsaturated lean clay. Experimental unsaturated soil mechanics. In: Proc. 2nd Int. Conf. on Unsaturated Soils. Weimar (Germany). pp. 445–452.

Romano, N., Brunone, B., Santini, A., 1998. Numerical analysis of one-dimensional unsaturated flow in layered soils. Adv. Water Resour. 21 (4), 315–324.

Schnaid, F., Consoli, N.C., Cumdani, R., Milititsky, J., 1995. Load-Settlement response of shallow foundations in structured unsaturated soils. In: Proc. 1st International Conference on Unsaturated Soils. Paris. pp. 999–1004.

Schuster, R.L., Highland, L., 2001. Socioeconomic and Environmental Impacts of Landslides in the Western Hemisphere. US Department of the Interior, US Geological Survey.

Sheng, D., 2011. Review of fundamental principles in modelling unsaturated soil behaviour. Comput. Geotech. 38 (6), 757–776.

Steenbergen, R.D.J.M., Geurts, C.P.W., van Bentum, C.A., 2009. Climate change and its impact on structural safety. HERON 54 (1).

Steensen-Bach, J.O., Foged, N., Steenfelt, J.S., 1987. Capillary induced stresses—fact or fiction? In: Proc. 9th European Conference on Soil Mechanics and Foundation Engineering. Hungary, Budapest. pp. 83–89.

Tariq, B.H., Miller, G.A., 2009. Shear strength of unsaturated soil interfaces. Can. Geotech. J. 46, 595–606.

Trenberth, K.E., 2011. Changes in precipitation with climate change. Clim. Res. 47, 123–138.

Turnbull, K.F., 2016. Transportation resilience: adaptation to climate change and extreme

weather events. Summary of the fourth EU–US Transportation research symposium. In: Proc. Transportation Research Board Conference. No. 53. Brussels, Belgium.
U.S. Department of Agriculture (USDA), 2016. Web Soil Survey. December. http://websoilsurvey.nrcs.usda.gov.
U.S. Geological Survey (USGS), 2016. National Water Information System: Web Interface. December. http://waterdata.usgs.gov/nwis/current/?type=gw&group_key=state_cd.
Vahedifard, F., Robinson, J.D., 2016. Unified method for estimating the ultimate bearing capacity of shallow foundation in variably saturated soils under steady flow. J. Geotech. Geoenv. Eng. https://doi.org/10.1061/(ASCE)GT.1943-5606.0001445.
Van Dam, J.C., Feddes, R.A., 2000. Numerical Simulation of Infiltration, Evaporation and Shallow Groundwater Levels With the Richards Equation. J. Hydrol. (Amst) 233, 72–85.
Van Genuchten, M.Th., 1980. A closed form equation for predicting the hydraulic conductivity of unsaturated soils. Soil Sci. Soc. Am. J. 44 (5), 892–898.
Vanapalli, S.K., Fredlund, D.G., Pufahl, D.E., Clifton, A.W., 1996. Model for the prediction of shear strength with respect to soil suction. Can. Geotech. J. 33, 379–392.
Vanapalli, S.K., Fredlund, D.G., 2000. Comparison of different procedures to predict unsaturated soil shear strength. Proc. the Conf. on Advances in Unsaturated Geotechnics (Geo-Denver) 195–209.
Vanapalli, S.K., Eigenbrod, K.D., Taylan, Z.N., Catana, C., Oh, W.T., Garven, E., 2010. A technique for estimating the Shaft resistance of test piles in unsaturated soils. Proc. 5th Int. Conf. on UNSAT 1209–1216.
Vanapalli, S.K., Oh, W.T., 2010a. A model for predicting the Modulus of elasticity of unsaturated soils using the soil-water characteristic curve. Int. J. Geotech. Eng. 4 (4), 425–433.
Vanapalli, S.K., Oh, W.T., 2010b. Interpretation of the bearing capacity of an unsaturated soils extending the effective and total stress approaches. Proc. 5th Int. Conf. on UNSAT 1223–1229.
Vanapalli, S.K., Taylan, Z.N., 2011a. Modeling the load carrying capacity of single piles in unsaturated soils using the modified α and the β methods. Proc. 13th Int. Conf. on IACMAG 599–607.
Vanapalli, S.K., Taylan, Z.N., 2011b. Model piles behavior in a compacted fine-grained unsaturated soil. Proc. 15th European Conf. on ESMGE 683–689.
Vanapalli, S.K., Taylan, Z.N., 2012. Design of single piles using the mechanics of unsaturated soils. Int. J. GEOMATE 2 (1), 197–204.
Vanapalli, S.K., Adem, H.H., 2013. A simple modeling approach for estimation of soil deformation behavior of natural expansive soils using the modulus of elasticity as a tool. In: Proc. 5th BIOT Conference on Poromechanics. Vienna, Austria. pp. 1695–1704.
Vardon, P.J., 2015. Climatic influence on geotechnical infrastructure: a review. Environ. Geotech. 2 (3), 166–174.
Warrick, A.W., 1991. Numerical approximations of Darcian flow through unsaturated soil. Water Resour. Res. 27 (6), 1215–1222.
Zaidel, J., Russo, D., 1992. Estimation of finite difference interblock conductivities for infiltration into initially dry soils. Water Resour. Res. 28, 2285–2295.
Zha, Y., Yang, J., Shi, L., Song, X., 2013. Simulating one-dimensional unsaturated flow in heterogeneous soils with water content-based richards equation. Vadose Zone J. 12 (2).
Zhang, F., 2010. Soil Water Retention and Relative Permeability for Full Range of Saturation. Pacific Northwest National Laboratory, Prepared for U.S. Department of Energy.